

# Electron energy-loss spectroscopy investigations of the electron density in $\text{ErMn}_2$ and $\text{ErMn}_2\text{D}_2$ compounds

T Galek<sup>1,2,4</sup>, C Hébert<sup>2</sup>, D Eyidi<sup>2</sup>, T Moskalewicz<sup>2,3</sup>, P Schattschneider<sup>2</sup>  
and H Figiel<sup>1</sup>

<sup>1</sup> Faculty of Physics and Applied Computer Science, AGH University of Science and Technology, Aleja Mickiewicza 30, PL-30059 Kraków, Poland

<sup>2</sup> Institute of Solid State Physics, Vienna University of Technology, Wiedner Hauptstrasse 8-10, A-1040 Vienna, Austria

<sup>3</sup> Faculty of Metallurgy and Material Science, AGH University of Science and Technology, Aleja Mickiewicza 30, PL-30059 Kraków, Poland

E-mail: [Tomasz.Galek@agh.edu.pl](mailto:Tomasz.Galek@agh.edu.pl)

Received 27 January 2005, in final form 5 May 2005

Published 27 May 2005

Online at [stacks.iop.org/JPhysCM/17/3657](http://stacks.iop.org/JPhysCM/17/3657)

## Abstract

Hydrogen atoms introduced into a bulk of rare earth–transition metal compound influence the electronic structure of the material. Additional electrons are expected to change the number of free electrons per volume unit present in the system. Electron energy-loss spectra were taken in the low-loss region up to 50 eV. In spectra for  $\text{ErMn}_2$  and  $\text{ErMn}_2\text{D}_2$  compounds, differences in the shape and position of the plasmon peak were observed. The dielectric functions were obtained from the energy-loss spectra using a Kramers–Kronig analysis. Different plasmon energies were found for both samples, and using the Drude model the numbers of free electrons per volume unit were calculated for pure and deuterated material. Significant differences were found, proving an increase of the free electron number per volume unit in the deuterated sample.

## 1. Introduction

The rare earth metals and their compounds easily absorb hydrogen, causing many changes of their physical properties, in particular structural and magnetic ones. These hydrides are interesting both for basic and applied research. Hydrogen causes a strong increase of the unit cell volume which for  $\text{YMn}_2\text{H}_x$  reaches about 30% [1]. Such an increase of the unit cell volume for Laves phase hydrides causes exceeding of the critical Mn–Mn distance important for localization of Mn magnetic moments and magnetic ordering [1–4]. The Laves phase type  $\text{RE}\text{Mn}_2$  compounds crystallize in cubic (C15) or hexagonal (C14) type structures [5]. The hydrides of cubic (C15) compounds have already been intensively investigated [1–5], whereas

<sup>4</sup> Address for correspondence: Institute of Solid State Physics, Vienna University of Technology, Wiedner Hauptstrasse 8-10, A-1040 Vienna, Austria.

**Table 1.** ErMn<sub>2</sub> and ErMn<sub>2</sub>D<sub>2</sub> cell characteristics at room temperature.

	ErMn <sub>2</sub>	ErMn <sub>2</sub> D <sub>2</sub>
Cell parameter, $a$ (Å)	5.297	5.666
Cell parameter, $c$ (Å)	8.469	9.068
Atoms per cell	12	20
Cell volume, $V_{\text{cell}}$ (Å <sup>3</sup> )	210.17	252.12
$n_a$ ( $10^{28}$ atoms m <sup>-3</sup> )	5.71	7.93

of the hydrides of the hexagonal type (*C*14) only SmMn<sub>2</sub>H<sub>2</sub> [6] and ErMn<sub>2</sub>H<sub>*x*</sub> [7] were reported recently.

Due to very high capacity, these materials are very attractive for hydrogen storage, as for example LaNi<sub>5</sub>.

One of the problems related with the above-mentioned properties is the behaviour of electrons introduced by hydrogen into the compound. Hydrogen atoms enter the interstitial positions in the lattice and their electrons enter the electronic band causing appropriate changes of the density of states [8].

Thus introduction of additional electrons into the crystal structure is expected to change the number of free electrons per volume unit. With respect to these effects the aim of this work was to investigate ErMn<sub>2</sub> and ErMn<sub>2</sub>D<sub>2</sub> samples using electron energy-loss spectroscopy (EELS) to find experimentally the differences of their electronic properties. Until now there have been no investigations of this type of hydride using EELS. EELS investigations showing shifts of plasmons due to hydrogen have been reported only for ZrH [9] and RE hydrides [10]. It was assumed that the replacement by deuterium does not influence the electronic properties of the system. Our investigations using electron energy-loss spectroscopy are focused on the low-loss region of the energy-loss spectrum, which contains information about the valence electron system. The obtained spectra were used for calculations of the number of free electrons per volume unit. Also the shape of the low-loss spectrum depends on the electronic properties of the material, and can be used for phase recognition [9, 10], and understanding the hydrogen-induced phenomena in ErMn<sub>2</sub> compound.

## 2. ErMn<sub>2</sub> and ErMn<sub>2</sub>D<sub>2</sub> compounds

The ErMn<sub>2</sub> and ErMn<sub>2</sub>D<sub>2</sub> compounds belong to the family of rare earth–transition metal compounds and their hydrides (deuterides). These compounds have a variety of interesting structural, electronic and magnetic properties. The bulk material of ErMn<sub>2</sub> can absorb hydrogen up to  $x = 4.3$  [7] per formula unit. Hydrogen introduced into the crystal structure is located in the interstitial sites of the A2B2 type. For intermediate hydrogen concentrations due to hydrogen atom interactions and diffusion, many structural and magnetic transformations take place with dependence on the temperature and hydrogen concentration [7].

The ErMn<sub>2</sub> and ErMn<sub>2</sub>H<sub>2</sub> compounds crystallize as the hexagonal *C*14 type Laves phase (*P*6<sub>3</sub>/*mmc* space group). The elementary unit cell of ErMn<sub>2</sub> compound consists of 4 atoms of Er and 8 atoms of Mn. The crystal structure of ErMn<sub>2</sub>D<sub>2</sub> compound is the same as that of ErMn<sub>2</sub>H<sub>2</sub>. The samples used in our experiment were the same as those used for neutron diffraction measurements [11]. The substitution of the H atoms with D atoms is essential for neutron scattering experiments due to the magnetic momentum of the D nucleus. Neutrons interact mainly with the nucleus of an atom and can feel the magnetic momentum.

All measurements were performed at room temperature for which the lattice parameters  $a$  and  $c$  were previously determined using x-ray diffraction measurements [11]; see table 1.

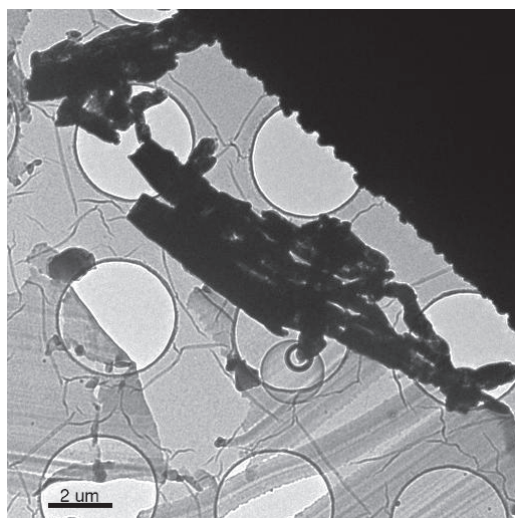


**Figure 1.** An overview of the specimen. The grey filaments are slices of epoxy resin. They are well separated from the compound grains.

The sample of  $\text{ErMn}_2$  was prepared from high purity materials using the induction melting technique and then annealed to obtain a well-defined single-phase material. Before deuterating, the material was checked by x-ray diffraction. After deuterating, the samples were annealed again at  $180^\circ\text{C}$  for a few hours to achieve phase equilibrium.

### 3. Specimen preparation

The powdered material was mixed with epoxy resin and then loaded into a 3 mm diameter brass tube and heated for 1 h at a temperature of  $150^\circ\text{C}$ . The whole procedure did not cause escape of deuterium from the sample. The next step was to grind the tube with a hardened epoxy to obtain a pin-like shape at one of the ends and cut it with an ultramicrotome with a diamond blade, that was set up to cut slices about 50 nm thick [12]. Then the sliced parts were placed on a supporting grid with a holey carbon substrate and were ready to use in the microscope. The average thickness of the specimen prepared this way was  $t/\lambda = 0.6$ , which fulfils the conditions necessary for the EELS experiment. Here  $t$  is the thickness and  $\lambda$  is the mean free path of an incident electron in the material. For EELS the value of  $t/\lambda$  should be in the range 0.4–0.8. Figure 1 shows the prepared sample. It can be seen that the pieces of our sample are not embedded in epoxy resin, which makes measurements much easier. Only the grains placed partly over vacuum were used for the analysis, which allowed us to avoid problems with carbon contamination.

Recorded spectra for the energy range appropriate for the oxygen K absorption edge showed that there was always oxygen present in the specimen, mostly related with surface oxides which made measurements very difficult. Further investigations showed that the material used for specimen preparation is mostly inhomogeneous, even within one grain. Quantitative microanalysis using the  $L_{2,3}$  absorption edge of Mn and  $N_{4,5}$  absorption edge of Er showed that atomic ratio 1:2 of Er to Mn is not always kept. Acquired diffraction patterns showed that the specimen is mostly a mixture of a crystalline and amorphous material.

Spectra presented in this publication were acquired only on the crystalline parts of the samples. For further analysis, spectra acquired from specimen with a thickness of

$t/\lambda = 0.4\text{--}0.8$  were chosen to avoid too large contribution from surface oxides. Surface losses only give a significant contribution to the energy-loss spectra for thinner specimens with  $t/\lambda < 0.3$ .

#### 4. EELS and dielectric functions

In combination with the methods available in the TEM for structural and crystallographic characterization, EELS in the electron microscope has been used extensively for chemical microanalysis. In the experiment, fast probe electrons interact with the specimen inelastically, losing energy by ionization of single atoms or other elementary excitations of the solid. What is actually measured is the double differential inelastic scattering cross section as a function of energy loss. In conventional TEM, energy filtering is routinely used for elemental mapping with spatial resolutions of better than 10 nm. With scanning electron probes, element-specific signals have been reported with atomic resolution [13, 14] or close to single atom detection [15, 16].

Whereas for ionization edges a quantum mechanical description of the cross sections is well adapted [17], the low-loss region is often described phenomenologically in terms of the energy-loss function. The reason is that here, both the initial and the final states of an excitation depend on the band structure, and electronic correlation plays a prominent role. The notorious difficulty to describe plasmons in the electron gas by a quantum approach is a direct consequence of this problem (see, e.g. [18] and references therein). It can be shown within classical electrodynamics [17] that the energy-loss function measures the imaginary part of the inverse dielectric function  $\varepsilon(\omega)$  where the energy loss relates to the frequency as  $E = \hbar\omega$ . When multiple scattering of the probe electron in the specimen can be neglected (or can be removed numerically), the single scattering distribution is [18]

$$S(E) = \frac{I_0 t}{\pi a_0 m_0 v^2} \operatorname{Im} \left[ \frac{-1}{\varepsilon(E)} \right] \ln \left[ 1 + \left( \frac{\beta}{\theta_E} \right)^2 \right] \quad (1)$$

where  $\varepsilon(E) = \varepsilon_1 + i\varepsilon_2$  is the complex dielectric function,  $I_0$  is the zero-loss intensity,  $t$  is the specimen thickness,  $v$  is the speed of the incident electron,  $m_0$  is the rest mass of an electron,  $a_0$  is the Bohr radius,  $\beta$  is the collection angle and  $\theta_E = E/(\gamma m_0 v^2)$  is the characteristic scattering angle for an energy loss  $E$ , where  $\gamma = 1/\sqrt{1 - v^2/c^2}$  is the relativistic correction factor. This important equation establishes a relationship between inelastic electron scattering and optical spectroscopy [19].

The real part of the complex dielectric function  $\varepsilon_1$  describes the polarizability of the electron system and the imaginary part  $\varepsilon_2$  is a measure for absorption occurring in the electron system. Using a Kramers–Kronig analysis one can obtain the dielectric functions from the experimental energy-loss function [17, 20]. Based on fact that the dielectric response is causal, the Kramers–Kronig transformation can be used to derive the function  $\operatorname{Re}[1/\varepsilon(E)]$  from  $\operatorname{Im}[-1/\varepsilon(E)]$ :

$$\operatorname{Re} \left[ \frac{1}{\varepsilon(E)} \right] = 1 - P \frac{2}{\pi} \int_0^\infty \operatorname{Im} \left[ \frac{-1}{\varepsilon(E')} \right] \frac{E' dE'}{E'^2 - E^2} \quad (2)$$

where  $P$  stands for the principal part of the integral, avoiding the pole at  $E' = E$ . To calculate  $\operatorname{Re}[1/\varepsilon(E)]$ , the energy-loss function has to be normalized by applying factor  $R_K$  to every channel of the spectrum.  $R_K$  is calculated by setting  $E = 0$  in equation (2), and we obtain

$$\operatorname{Re} \left[ \frac{1}{\varepsilon(0)} \right] = 1 - \frac{2}{\pi R_K} \int_0^\infty \operatorname{Im} \left[ \frac{-1}{\varepsilon(E)} \right] \frac{dE}{E} \quad (3)$$

since  $\text{Re}[1/\varepsilon(0)] = \varepsilon_1/(\varepsilon_1^2 + \varepsilon_2^2)$ , the  $\varepsilon_1$  and  $\varepsilon_2$  become very large for a metal when  $E \rightarrow 0$ , thus  $\text{Re}[1/\varepsilon(0)] = 0$  [17]. After retrieving  $\text{Re}[1/\varepsilon(E)]$  the dielectric functions can be calculated as follows:

$$\varepsilon_1 = \frac{\text{Re}[1/\varepsilon]}{(\text{Re}[1/\varepsilon])^2 + (\text{Im}[-1/\varepsilon])^2} \quad (4)$$

$$\varepsilon_2 = \frac{\text{Im}[-1/\varepsilon]}{(\text{Re}[1/\varepsilon])^2 + (\text{Im}[-1/\varepsilon])^2}. \quad (5)$$

Using the obtained dielectric functions, the effective number of electrons contributing to energy losses up to energy  $E$  per atom can be calculated [17]:

$$N_{\text{atom}}(E) = \frac{2\varepsilon_0 m_0}{\pi \hbar^2 e^2 n_a} \int_0^E E' \varepsilon_2(E') dE' \quad (6)$$

where  $n_a$  is the number of atoms per unit volume. Using the unit cell parameters of the ErMn<sub>2</sub> and ErMn<sub>2</sub>D<sub>2</sub> compounds (table 1), the value of  $n_a$  can be calculated. However, in the case of materials containing hydrogen it is more convenient to show the effective number of electrons contributing to energy losses up to energy  $E$  per unit cell:

$$N_{\text{cell}}(E) = \frac{2\varepsilon_0 m_0}{\pi \hbar^2 e^2 (V_{\text{cell}})^{-1}} \int_0^E E' \varepsilon_2(E') dE'. \quad (7)$$

Another quantity which can be determined is the plasmon energy  $E_p$ , defined as the energy where  $\varepsilon_1(E)$  passes through zero with positive slope  $\varepsilon_1(E_p) = 0$  [17, 20]. Because the plasmon energy according to the Drude theory is given by the relation:

$$E_p^2 = \frac{n_f \hbar^2 e^2}{\varepsilon_0 m}, \quad (8)$$

we can calculate  $n_f$ , which is the number of free electrons per volume unit. The number of free electrons per crystal cell  $n_c$  can be calculated by multiplying  $n_f$  by the volume of the unit cell  $V_{\text{cell}}$  (table 1).

## 5. The experiment and results

All measurements presented in this work were performed using an analytical 200 kV transmission electron microscope FEI TECNAI F20 S-TWIN with Schottky emitter as a gun source, and equipped with a Gatan imaging filter. All spectra were recorded in STEM mode with 0.05 eV/channel dispersion in the energy range up to 50 eV with a collection angle of the spectrometer 8 mrad.

Due to magnetic instabilities inside the TEM column and inside the spectrometer, spectra acquired with a longer acquisition time had a worse resolution. These magnetic instabilities cause shifts in the energy scale of the energy-loss spectrum, broadening all of its features.

The resolution of each spectrum was determined by measuring the full width at half-maximum (FWHM) of the zero-loss peak (ZLP), and reached 0.9–1.2 eV. To improve the resolution of EELS spectra the acquisition time was set to a value ranging from 0.05 to 0.2 s. However, while recording spectra with a shorter time of acquisition, we lose the intensity. To compensate for this effect, 200–1000 spectra at every investigated point were recorded. For further processing, selection of the spectra was done taking into account only spectra with the best resolution (smallest FWHM). Afterwards, selected spectra were aligned according to the position of the ZLP and added. That procedure allowed us to obtain fine spectra with a resolution of 0.65 eV FWHM of the ZLP.

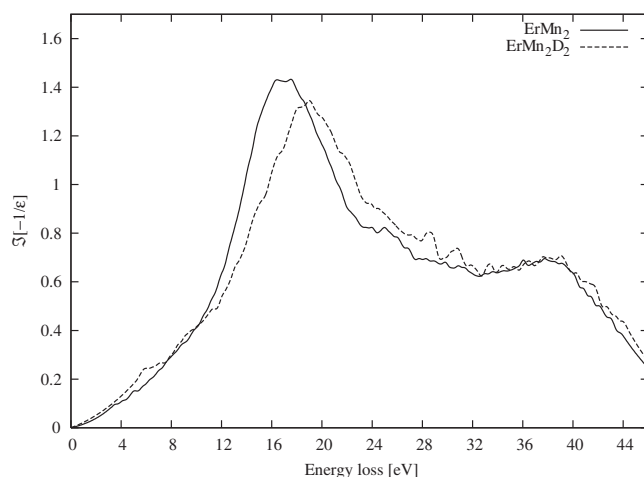


**Figure 2.** Energy-loss functions for  $\text{ErMn}_2$  and  $\text{ErMn}_2\text{D}_2$ .

**Table 2.** The plasmon energies and the number of free electrons obtained for  $\text{ErMn}_2$  and  $\text{ErMn}_2\text{D}_2$  compounds.

	$\text{ErMn}_2$	$\text{ErMn}_2\text{D}_2$
$E_p$ (eV)	15.3	15.5
$n_f$ ( $10^{28} \text{ m}^{-3}$ )	16.97	17.42
$n_c$ (1/cell)	35.67	43.92

Acquired spectra  $S_{\text{exp}}(E)$  were Fourier-log deconvoluted to obtain the single scattering distribution  $S(E)$  as described in [17]. Due to the limited energy resolution the deconvoluted spectra could not be applied directly. After the deconvolution process the spectra in the range from 0 to 3–5 eV were extrapolated using an exponential fit. One has to be very careful during this procedure because small changes in the energy-loss spectra in this energy range cause large variations in calculated  $\varepsilon_1$  and  $\varepsilon_2$  functions. Afterwards the spectra were normalized to obtain the energy-loss function  $\text{Im}[-1/\varepsilon(E)]$  which was used to calculate the real and imaginary parts of the dielectric function.

During our experiments many spectra were recorded on a few samples of  $\text{ErMn}_2$  and  $\text{ErMn}_2\text{D}_2$  compounds to prove the repeatability of the experiment. However, only two spectra were chosen to present in this publication because of the best resolution, only 0.65 eV FWHM of the ZLP in both cases. Also both spectra have a negligible noise signal which allows us to see the fine structure of the low energy-loss spectra.

The energy-loss functions for both pure  $\text{ErMn}_2$  and deuterated  $\text{ErMn}_2\text{D}_2$  material are shown in figure 2. A shift of the plasmon peak is clearly visible. For  $\text{ErMn}_2$  the plasmon peak is at 17 eV and for  $\text{ErMn}_2\text{D}_2$  it is shifted by 1.6 eV and is at 18.6 eV. Differences in the positions of the plasmon peak and the shape of the spectra in the low-loss region allows phase identification by fingerprinting.

The real and imaginary parts of the dielectric functions are shown in figure 3. Using the obtained  $\varepsilon_1(E)$ , the plasmon energies,  $E_p$ , were determined for both compounds, and numbers of free electrons per volume unit  $n_f$  and unit cell  $n_c$  were calculated; these are presented in table 2.

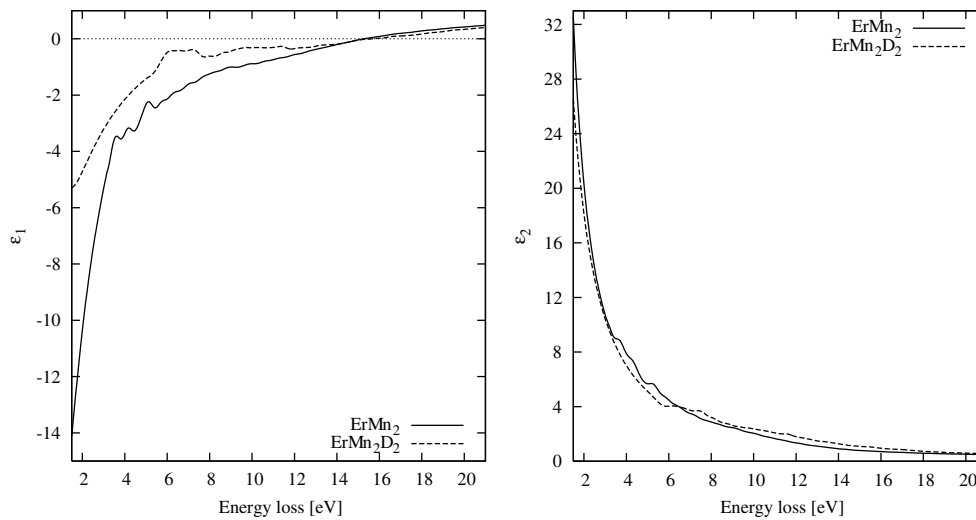


**Figure 3.** The dielectric functions  $\epsilon_1(E)$  and  $\epsilon_2(E)$  for  $\text{ErMn}_2$  and  $\text{ErMn}_2\text{D}_2$ .

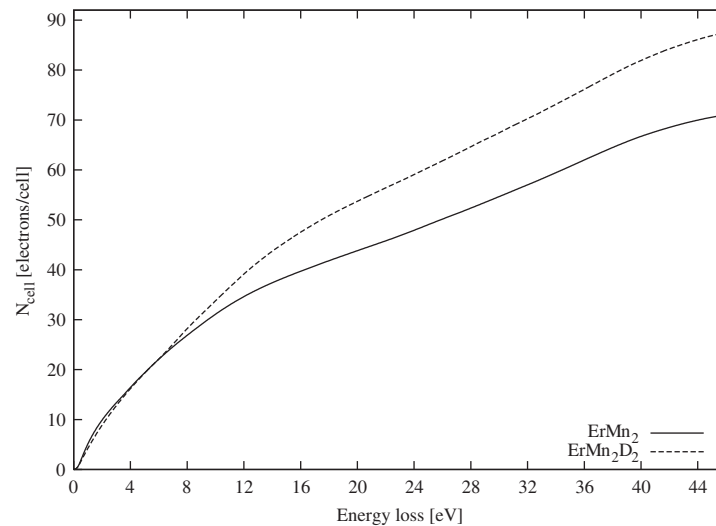


**Figure 4.**  $N_{\text{cell}}(E)$  dependences for  $\text{ErMn}_2$  and  $\text{ErMn}_2\text{D}_2$ .

Having the  $\epsilon_2(E)$  function, the effective numbers of electrons contributing to energy losses up to energy  $E$  per unit cell  $N_{\text{cell}}(E)$  were calculated, and they are presented in figure 4. A pronounced difference of the curves for pure and deuterided samples is visible.

## 6. Conclusions

The plasmon energies  $E_p$  for pure and deuterided samples allowed us to calculate the  $n_f$  values which are proportional to  $E_p^2$ , as presented in table 2. The resultant value of  $n_c$  for  $\text{ErMn}_2$  is then 35.67, which corresponds very well to the expected number of 36 electrons, because in the unit cell of  $\text{ErMn}_2$  there are 4 atoms of Er and 8 atoms of Mn, which gives  $\approx 3$  free electrons

per atom. Also for  $\text{ErMn}_2\text{D}_2$  the experimental value 43.92 corresponds well to the expected number of 44 electrons per unit cell obtained with assumption that each D atom contributes one electron to the system. This means that the hydrogen is indeed giving its electron to the electron band, as was expected.

### Acknowledgments

The authors express their gratitude for the support of the Austrian Science Foundation, project P14038-PHY and the Polish Committee for Scientific Research.

### References

- [1] Figiel H, Przewoźnik J, Paul-Boncour V, Lindbaum A, Gratz E, Latroche M, Escorne M, Percheron-Guégan A and Mietniowski P 1998 *J. Alloys Compounds* **274** 29–37
- [2] Zukrowski J, Figiel H, Budziak A, Zachariasz P, Fischer G and Dormann E 2002 *J. Magn. Magn. Mater.* **238** 129–39
- [3] Figiel H, Budziak A, Zukrowski J, Fischer G, Kelemen M T and Dormann E 2002 *J. Alloys Compounds* **335** 48–58
- [4] Goncharenko I N, Mirebeau I, Irodova A V and Suard E 1999 *Phys. Rev. B* **59** 9324–31
- [5] Wiesinger G 1991 *Handbook of Magnetic Materials* vol 6, ed K H J Buschow (Amsterdam: Elsevier Science B.V.) chapter 6 (Magnetism of Hydrides)
- [6] Figiel H, Kapusta Cz, Budziak A and Riedi P C 2002 *J. Alloys Compounds* **330–332** 361–4
- [7] Figiel H, Budziak A, Zachariasz P, Zukrowski J, Fischer G and Dormann E 2004 *J. Alloys Compounds* **368** 260–8
- [8] Pajda M, Ahuja R, Johansson B, Wills J M, Figiel H, Paja A and Eriksson O 1996 *J. Phys.: Condens. Matter* **8** 3373–84
- [9] Zaluzek N 1992 *Transmission Electron Energy Loss Spectrometry in Materials Science* ed M M Disko, C C Ahn and B Fultz (Warrendale, PA: Minerals, Metals and Materials Society) pp 241–66
- [10] Colliex C, Gasgnier M and Trebbia P 1976 *J. Physique* **37** 397–406
- [11] Budziak A 2002 Hydrogen influence on physical properties of selected rare earth–manganese compounds *PhD* AGH University of Science and Technology, Kraków
- [12] Williams D B and Carter C B 1996 *Transmission Electron Microscopy: A Textbook for Materials Science* (New York: Plenum)
- [13] Batson P E 1993 Simultaneous STEM imaging and electron energy-loss spectroscopy with atomic-column sensitivity *Nature* **366** 727–8
- [14] Bleloch A, Falke U and Falke M 2003 *Microscopy-and-Microanalysis* vol 9 (Berlin: Springer) pp 40–1
- [15] Krivanek O, Mory C, Tenc M and Colliex C 1991 *Microsc. Microanal. Microstruct.* **2** 257–67
- [16] Vanfleet R, Muller D A, Gossmann H J, Citrin P H and Silcox J 2001 Atomic-scale imaging of dopant atom distributions within silicon delta-doped layers *Advances in Materials Problem Solving with the Electron Microscopy (Symp.—Materials-Research-Society-Symp.-Proc.)* (Warrendale, PA: Materials Research Society)
- [17] Egerton R F 1986 *Electron Energy Loss Spectroscopy in the Electron Microscope* (New York: Plenum)
- [18] Schattschneider P and Jouffrey B 1995 Plasmons and related losses *Energy-Filtering Transmission Electron Microscopy* ed L Reimer (Berlin: Springer) pp 151–224
- [19] Ingram J C, Nebesny K W and Pemberton J E 1990 *Appl. Surf. Sci.* **44** 279–91
- [20] Schattschneider P 1986 *Fundamentals of Inelastic Electron Scattering* (Wien: Springer)